Eur. Phys. J. E (2006)
DOI 10.1140/epje/i2005-10080-0

THE EUROPEAN PHYSICAL JOURNAL E

# Confinement-induced instability and adhesive failure between dissimilar thin elastic films

J.Y. Chung[1], K.H. Kim[1], M.K. Chaudhury[1,a], J. Sarkar[2], and A. Sharma[2]

[1] Department of Chemical Engineering, Lehigh University, Bethlehem, PA 18015, USA
[2] Department of Chemical Engineering, Indian Institute of Technology, Kanpur, India

Received 19 November 2005 and Received in final form 13 February 2006 /
Published online: 11 May 2006 – 

**Abstract.** When two thin soft elastomeric films are separated from each other, an elastic instability develops at the interface. Although similar instability develops for the case of a soft film separating from a rigid adherent, there are important differences in the two cases. For the single-film case, the wavelength of instability is independent of any material properties of the system, and it scales only with thickness of the film. For the two-film case, a co-operative instability mode develops, which is a non-linear function of the thicknesses and the elastic moduli of both films. We investigate the development of such instability by energy minimization procedures. Understanding the nature of this instability is important, as it affects the adhesive compliance of the system and thus the energy release rate in the debonding of soft interfaces.

**PACS.** 68.35.-p Solid surfaces and solid-solid interfaces: Structure and energetics – 68.35.Gy Mechanical properties; surface strains – 68.35.Np Adhesion

## 1 Introduction

When a thin elastic film is separated from a rigid flat surface, its surface loses its planarity and subsequently evolves to a fingering [1–3] or a worm-like pattern [4,5] with a fairly regular spacing. The wavelength ($\lambda$) of this instability varies linearly only with the thickness $h$ [1–6], but depends on no other property of the film. Studying the properties of these pattern formations in elastic systems is valuable, as it has been found recently that the cavitation that grows as a result of elastic instability is fundamental to understanding the nucleation and growth of crack of soft materials in confined geometries [1–12]. Parallels to the cavitation seen with these elastic systems have also been discovered in some recent interesting experiments with purely viscous liquids in confined geometries [13,14].

In the case of a single thin film bonded to a rigid support contacting or separating a rigid adherent, the elastic instability is the direct result of the shear deformation in the film. For an interfacial perturbation with a finite amplitude, the energy stored in the film diverges in the limit of infinitely long and vanishingly small wavelengths, but has a minimum at a critical wavelength. Since the net elastic deformation is a direct consequence of the displacements of the film parallel and perpendicular to the interface, the energy minimization does not involve the film modulus. Only length scale of the problem is the film thickness, which determines the wavelength of instability. What happens when the bonded thin film contacts to and then separates from another thin compliant film on a rigid support? In this case, we need to consider the coupled deformations in both the films for a given surface perturbation [15–17]. Since the energies in the two films now have to be minimized for a common wavelength, the vertical and parallel displacements of both the films are non-linearly coupled to each other. Intuitively, there would be a co-operative instability mode that minimizes the total elastic energies of the films simultaneously; thus one would expect that the wavelength would be dependent on the material properties of both the films in a non-linear way. Thus, the exclusive dependence of the wavelength on the film thickness as evidenced for a single film cannot be expected for the case with two films and the problem has to be solved more rigorously. In what is described below, we tackle the problem in two ways. In the first case (*Case I*), we determine the scaling relation for the wavelength with the modulus and the thickness of the two films by considering the "separation" of the two films from intimate contact. In the second case (*Case II*), we study the "approach" of the two films towards each other. In the latter case, the surfaces of the films undergo undulations as soon as the stiffness of the adhesive (for example, van der Waals) force acting across the films overcomes the elastic stiffness of the films. This happens even before the two surfaces come into intimate molecular contact, as shown by the linear stability analysis of two approaching

[a] e-mail: mkc4@lehigh.edu

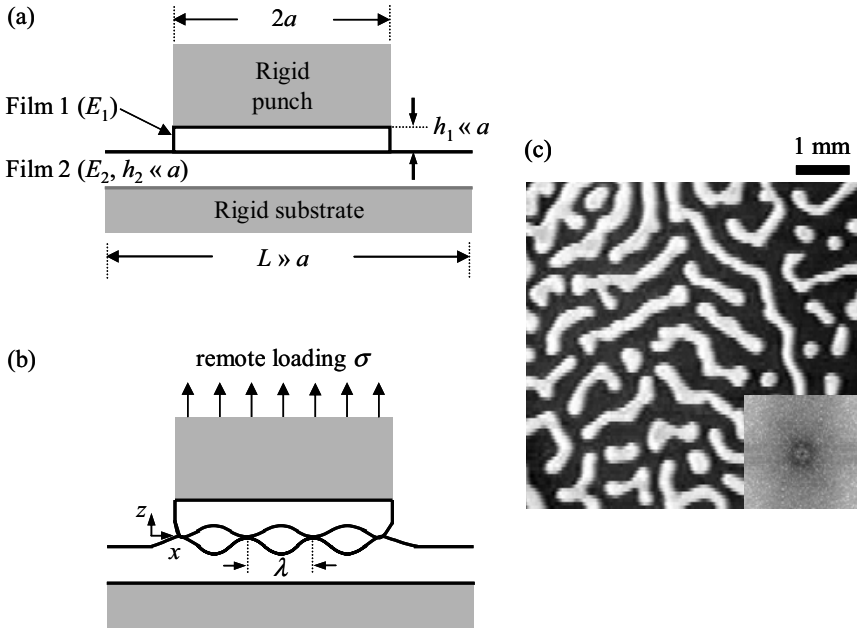


**Fig. 1.** Schematic illustration of a confinement-induced instability between two elastic films in an axisymmetric probe tack configuration. (a) The initial state where a rigid cylindrical punch having a thin elastic film (denoted by film 1) below it is adhered onto another film (denoted by film 2) fixed at a rigid substrate. The lateral length scale $a$ significantly exceeds the thicknesses of the films. The physical properties of both films may widely differ from each other. (b) The wrinkled state: when subjected to a normal load, the confined films deform with undulating patterns which have a characteristic wavelength $\lambda$. (c) A typical image of the worm-like patterns observed in an optical microscope (bright regions indicate areas detached from the substrate) and the corresponding two-dimensional FFT spectrum (inset to figure). The symmetric ring on the FFT image corresponds to the dominant wavelength of the patterns, and the symmetry of the spectrum reflects the fact that the patterns are distributed isotropically. Experimental parameters are $h_1 = 190\,\mu$m, $E_1 = 2.7\,$MPa, $h_2 = 130\,\mu$m, and $E_2 = 1.3\,$MPa, and the resulting wavelength $\lambda = 610\,\mu$m.

surfaces [1,7]. We then compare this prediction with the instability wavelengths obtained from two different experiments. The analysis obtained from the *Case I* version of the theory allows us to obtain a scaled thickness of the two films in terms of their physical properties, with respect to which both the experimental data and theoretical predictions were compared. Finally, we show how the information about these instabilities can be used to account for the forces needed to pull off two such films from close contact.

## 2 Co-operative instability in two soft films

For *Case I*, we consider a model system, where a circular, thin elastomeric film bonded to a flat-ended cylindrical probe is separated from another thin film bonded to another rigid substrate (Fig. 1a). These films are made of crosslinked poly(dimethylsiloxane) (PDMS) of various elastic moduli. Because of their elastomeric properties, these films are effectively incompressible materials (*i.e.*, Poisson ratio $\approx 0.5$), exhibiting linear elastic behavior at low enough strains. We consider that the specimens are loaded in plain strain. Furthermore, we consider that the pull-off of a circular thin film from a rigid substrate and that of a cylindrical rigid punch from a thin film are symmetric. This is a good approximation when $a/h_1 \gg 1$ and $a/h_2 \gg 1$. Under an applied stress, we consider that the two surfaces of the films (at $z = 0$) undergo sinusoidal perturbations $u_{1,z}(x) = \delta_1 \cos(2\pi x/\lambda)$ and $u_{2,z}(x) = \delta_2 \cos(2\pi x/\lambda)$, where $u_{1,z}$ and $u_{2,z}$ are the displacements of the films in the $z$-direction and $\delta_1$ and $\delta_2$ are the amplitudes of the perturbations in the films. Here and elsewhere 1 and 2 in the subscripts denote the upper film and lower film, respectively. When subjected to an applied load or attractive inter-surface interactions of a critical strength [1,7], both films become unstable and form an isotropic undulating pattern of wavelength $\lambda \ll a$, which spans the entire surface of the films (Figs. 1b-c). These patterns arise as the films cannot stretch in the normal direction with the concomitant lateral Poisson contraction. Thus, shear deformations must develop in the $x$ and $z$ directions (Fig. 1b) of the interface causing the roughening of the interface. During debonding, the wavelength of the instability remains virtually unchanged, with its amplitude growing gradually until separation occurs. Previous theoretical works also show that although a small vertical amplitude pattern first forms during a close ($\sim 10\,$nm) approach of the surfaces due to the surface instability [1,7, 16,17], the pattern length scale remains largely unchanged during a closer approach of the surfaces, as well as during debonding [18,19].

The total energy of the system is given by the sum of three contributions: the elastic strain energy $\overline{U}_E$ of the films, the work of adhesion $W_a$, and the surface energy $\overline{U}_S$

of the undulated films. However, the adhesion energy effect is neglected here, as it is relatively unimportant in the fact that the interaction energy is conceptually independent of the wavelength of the instability. Thus, the total energy $\overline{U}_T$ (energy/area) consists of the elastic strain energy and the surface energy [1,7]:

$$\overline{U}_T \sim \sum_{i=1,2} E_i h_i \left[ \left( \frac{\partial u_{i,z}}{\partial x} \right) + \left( \frac{\partial u_{i,x}}{\partial z} \right) \right]^2 + \sum_{i=1,2} \gamma_i \left( \frac{\partial u_{i,z}}{\partial x} \right)^2, \quad (1)$$

where $E_i$, $h_i$, and $\gamma_i$ are the modulus, thickness, and surface tension of films 1 and 2 ($i = 1, 2$), and $u_{i,x}$ and $u_{i,z}$ are the components of the displacement field of the corresponding films in the $x$ and $z$ directions (a local Cartesian coordinate is denoted in Fig. 1b). The contribution of the surface energy in equation (1) is very small for elastomers of thickness in the range of micrometers as compared to that of the elastic energy (*i.e.*, $\gamma_i/E_i h_i < 1$), specifically in physical systems where such instabilities are engendered. Thus, we neglect the second term of equation (1) in comparison to the strain energy terms. Taking the characteristic length scales as $\lambda$ and $h_i$ along the $x$ and $z$ axes, the amplitude of the perturbation in each film as $\delta_i$, and considering longitudinal and transverse shear strains in both the films, equation (1) in conjunction with the displacement continuity equation ($\partial u_{i,x}/\partial x + \partial u_{i,z}/\partial z = 0$) can be written as

$$\overline{U}_T \sim E_1 h_1 \delta_1^2 \left( \frac{1}{\lambda} + \frac{\lambda}{h_1^2} \right)^2 + E_2 h_2 \delta_2^2 \left( \frac{1}{\lambda} + \frac{\lambda}{h_2^2} \right)^2. \quad (2)$$

To find the length scale of the problem, the main task lies in minimizing $\overline{U}_T$ with respect to $\lambda$. However, before such minimization is attempted, we need a relationship between $\delta_1$ and $\delta_2$, which can be accomplished by balancing the stresses in the modulated films. These stresses can be obtained by taking the partial derivatives of $\overline{U}_T$ with respect to $\delta_1$ and $\delta_2$ and setting them to equal, *i.e.*,

$$E_1 h_1 \delta_1 \left( \frac{1}{\lambda} + \frac{\lambda}{h_1^2} \right)^2 = E_2 h_2 \delta_2 \left( \frac{1}{\lambda} + \frac{\lambda}{h_2^2} \right)^2. \quad (3)$$

Within the long-scale approximation, *i.e.*, $\lambda > h_1, h_2$, equation (3) reduces to

$$\frac{E_1 \delta_1}{h_1^3} \sim \frac{E_2 \delta_2}{h_2^3}. \quad (4)$$

Substitution of equation (4) in equation (2) leads to the following expression for the total elastic energy at a given composite amplitude $\delta$ ($= \delta_1 + \delta_2$) of the films:

$$\overline{U}_T \sim \frac{E_1 E_2 \delta^2}{\left(E_1 h_2^3 + E_2 h_1^3\right)^2} \left[ E_2 h_1^7 \left( \frac{1}{\lambda} + \frac{\lambda}{h_1^2} \right)^2 + E_1 h_2^7 \left( \frac{1}{\lambda} + \frac{\lambda}{h_2^2} \right)^2 \right]. \quad (5)$$

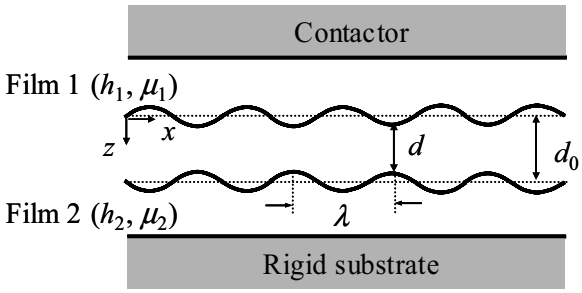


**Fig. 2.** Contact mode of two elastic films of thicknesses $h_1$ and $h_2$ and shear moduli $\mu_1$ and $\mu_2$ bonded to contactor and rigid substrate, respectively. Surface roughening at the interface of both the films is engendered as the initial separation distance $d_0$ is below a critical value.

Minimization of $\overline{U}_T$ with respect to $\lambda$ at a constant $\delta$ yields

$$\lambda \sim \left( \frac{E_1 h_2^7 + E_2 h_1^7}{E_1 h_2^3 + E_2 h_1^3} \right)^{1/4}. \quad (6)$$

We have checked the validity of equation (6), and thus the long-scale approximation, by numerically evaluating the minimum energy $\overline{U}_T$ after combining equations (2, 3). Within the range of the thicknesses of the films and their elastic moduli used in our experiments, numerical analysis shows that, for a given $\delta$, there exist one positive and one negative real root of $\lambda$, all the other roots being pairs of complex conjugates. The positive real value of $\lambda$, thus obtained, differs by only about 1% from the solution of equation (6). Thus, we will, henceforth, treat the right-hand side of equation (6) as the scaled thickness for two films.

It can be noted that equation (6) reduces to $\lambda \sim h_1$ (or $h_2$) when one of the films is infinitely rigid compared to the other or one of the substrates does not have a thin film on it (*i.e.*, $E_1$ (or $E_2$) $\to \infty$ or $h_1$ (or $h_2$) $\to 0$), consistent with the case of an elastic film interacting with a rigid body. Previous studies establish the proportionality factor between $\lambda$ and $h$ to be $\sim 4$ [1,3].

For *Case II*, we now consider the "approach" and the instability of two films bonded to two rigid substrates (Fig. 2). When the separation distance declines below a critical value $d_c$, the adhesive interactions become strong enough to trigger an elastic instability at the interfaces. The surface becomes rough as depicted schematically in Figure 2. To obtain the length scale of instability, the total energy is minimized [16,17] with respect to the displacements in the films. The total energy of the deformed films is composed of the elastic and the adhesive energy:

$$U_T = \int_V W(\boldsymbol{\varepsilon}) \mathrm{d}V + \int_S U_A(d) \mathrm{d}S, \quad (7)$$

where $W(\boldsymbol{\varepsilon})$ is the strain energy density and $\boldsymbol{\varepsilon}$ is the strain tensor in the films. For incompressible elastic films, $W(\boldsymbol{\varepsilon}) = \frac{\mu_1}{2} \boldsymbol{\varepsilon} : \boldsymbol{\varepsilon}$ in film 1 and similarly $\frac{\mu_2}{2} \boldsymbol{\varepsilon} : \boldsymbol{\varepsilon}$ in film 2. $U_A$ is the inter-surface interaction potential per unit area. Its value is dependent on the inter-surface separation distance $d$ and can have any general form, including the short-range

van der Waals interactions and the long-range electrostatic force. For a linear stability analysis, the interaction potential is linearized and expanded in a power series keeping terms up to quadratic order in $(\boldsymbol{u}_1 - \boldsymbol{u}_2)\cdot\boldsymbol{n}$,

$$U_A(d) = U_0 + F\big((\boldsymbol{u}_1 - \boldsymbol{u}_2)\cdot\boldsymbol{n}\big) + \frac{Y}{2}\big((\boldsymbol{u}_1 - \boldsymbol{u}_2)\cdot\boldsymbol{n}\big)^2, \quad (8)$$

where $d = d_0 - ((\boldsymbol{u}_1 - \boldsymbol{u}_2)\cdot\boldsymbol{n})$ is the inter-surface gap distance, $\boldsymbol{u}_1$, $\boldsymbol{u}_2$ being the displacement fields in films 1 and 2. The Taylor series expansion coefficients can be expressed in terms of the various derivatives of the interaction energy,

$$U_0 = U_A\big(d_0\big), \qquad F = U_A'\big(d_0\big), \qquad Y = U_A''\big(d_0\big). \quad (9)$$

The equilibrium displacement fields of the films which minimize the total energy must satisfy the rigid boundary conditions at the respective film-substrate interfaces ($\boldsymbol{u}_1(x,-h_1) = 0$; $\boldsymbol{u}_2(x, d_0 + h_2) = 0$), and the traction boundary conditions at the common interface

$$\begin{aligned}
&\sigma_{1,xz}(x,0) = 0,\\
&\sigma_{1,zz}(x,0) = -\big\{F + Y\big[u_{1,z}(x,0) - u_{2,z}(x,d_0)\big]\big\},\\
&\sigma_{2,xz}(x,0) = 0,\\
&\sigma_{2,zz}(x,0) = -\big\{F + Y\big[u_{1,z}(x,0) - u_{2,z}(x,d_0)\big]\big\}. \quad (10)
\end{aligned}$$

Since both films are incompressible, the homogeneous solution has displacements vanishing everywhere in both films, and the stress state in both films is one of constant pressure (equal to $-F$). To consider inhomogeneous displacements, the homogeneous solution is perturbed with bifurcation fields of the form $u^*_{1,z}(x,0) = \alpha\cos(kx)$ and $u^*_{2,z}(x,d_0) = \beta\cos(kx)$ such that the normal stresses at the interface have the form $\sigma^*_{1,zz}(x,0) = -Y[u^*_{1,z}(x,0) - u^*_{2,z}(x,d_0)]$ and $\sigma^*_{2,zz}(x,d_0) = -Y[u^*_{1,z}(x,0) - u^*_{2,z}(x,d_0)]$, where $*$ in the superscripts denotes inhomogeneous deformation. A film with sinusoidal displacement field satisfying the stress equilibrium condition $\boldsymbol{\nabla}\cdot\boldsymbol{\sigma} = 0$ at the bulk and the rigid and stress-free boundary conditions at the surface gives

$$\begin{aligned}
\sigma_{1,zz}(x,0) &= 2\mu_1 S\big(kh_1\big)\cos(kx),\\
\sigma_{2,zz}(x,d_0) &= 2\mu_2 S\big(kh_2\big)\cos(kx), \quad (11)
\end{aligned}$$

where $S(\xi) = [1 + \cosh(2\xi) + 2\xi^2]/[\sinh(2\xi) - 2\xi]$.

Equations (10, 11) give the relation between the interaction stiffness $Y$ as defined in equation (9) and other physical parameters of the system:

$$-Y = \frac{2k\mu_1\mu_2 S\big(h_1k\big)S\big(h_2k\big)}{\mu_1 S\big(h_1k\big) + \mu_2 S\big(h_2k\big)}\,. \quad (12)$$

Any non-trivial solution of the above equation for the wave number $k$ ($= 2\pi/\lambda$) gives the periodic inhomogeneous deformation field for the interfaces. The lowest value of $-Y$ for which bifurcation is possible is the critical interaction stiffness denoted by $-Y_c$. The corresponding wave number is the critical mode denoted by $k_c$. This is the wavelength that is observed in experiments at the onset of instability as the films are made to approach each other very closely ($\sim$ 10 nm). At this time, the vertical amplitude of the resulting structures is also very small. However, the linear bifurcation approach is not valid during the pull-off or debonding phase when the vertical amplitude increases. In this phase, non-linear simulations [18,19] based on energy minimization of patterns showed the following features. 1) A complete debonding occurs at distances far greater than the distance at the onset of instability, which is due to the metastability or pinning of instability in a local minimum of the energy; 2) the wavelength of patterns remains largely robust during debonding because the number of structures per area remains unaltered, only the contact areas shrink with increasing inter-surface distance.

In the above linear stability analysis, the films can also be viewed as a two-spring model in series, and the total stiffness of the films $K_{eff}$ is thus given by

$$\frac{1}{K_{eff}} = \frac{h_1}{\mu_1} + \frac{h_2}{\mu_2} = \frac{h}{\mu^*}\,, \quad (13)$$

where $h$ ($= h_1 + h_2$) and $\mu^*$ represent the total thickness and the effective shear modulus, respectively. Non-dimensionalization introduces three parameters $M_1$, $M_2$, and $H$ such that $M_1 = \mu_1/\mu^*$, $M_2 = \mu_2/\mu^*$, $H = h_1/h$, and $1-H = h_2/h$. Then, equation (12) in non-dimensional form is

$$\frac{-Y}{K_{eff}} = \frac{2qM_1M_2S(Hq)S\big[(1-H)q\big]}{\big\{M_1S(Hq) + M_2S\big[(1-H)q\big]\big\}}\,, \quad (14)$$

where the non-dimensional wave number $q = hk$. For particular values of $H$, $M_1$, and $M_2$ as obtained from the individual values of $h_1$, $h_2$, $\mu_1$, and $\mu_2$, the value of $q_c$ is sought for which $-Y_c$ is a minimum. This is the length scale observed at the interface as will be discussed in the context of Figure 5.

## 3 Experimental studies of instability

In order to test the above predictions of the elastic instability at the interface of two films, we performed the punch pull-off experiment [5] (which is the basis of all the above theoretical derivations), as well as an asymmetric double cantilever beam (ADCB) test [1,3] (see Fig. 3). Although the detailed mechanics of the ADCB experiment is different from that of the punch test, we reason that as the wavelength of the instability is primarily due to the minimization of the elastic energies of the two thin soft films, the two systems would exhibit similar behavior. The punch pull-off experiment was carried out by contacting a thin PDMS film supported on a rigid circular glass disc (radius 5 mm) to another PDMS film supported on a rigid glass slide. As the disc was separated from the glass plate in a pull-off mode using a nanomotion controller, small cavitation bubbles developed at the interface, which finally evolved into a fully developed instability pattern just before the disc separated from the flat plate. The pull-off forces were measured, and the instability patterns

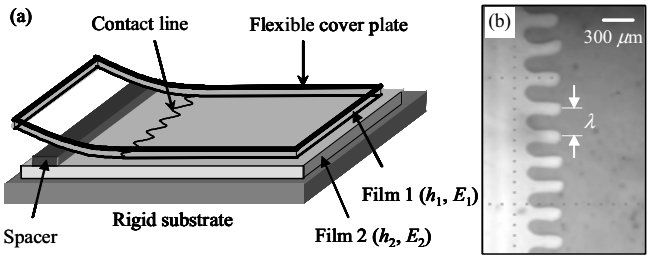


**Fig. 3.** (a) Schematic of an asymmetric double cantilever beam (ADCB) experiment in which a thin elastic film (denoted by film 1) bonded to a flexible glass cover plate (flexural rigidity $D \approx 0.02\,\mathrm{Nm}$) is brought into contact with another thin elastic film (denoted by film 2) fixed at a rigid glass substrate (flexural rigidity $D \approx 6\,\mathrm{Nm}$). A spacer of height $100\,\mu\mathrm{m}$ is inserted in-between the films to open the crack. In a critically confined geometry of films, the straight contact line becomes undulatory and forms a fingering pattern with a well-defined characteristic wavelength $\lambda$. (b) A typical video micrograph of instabilities observed in an optical microscope (the bright region on the left side of the image represents the area where the two surfaces are not in contact). In this image, the measured wavelength $\lambda = 340\,\mu\mathrm{m}$. The upper film and lower film had $h_1 = 95\,\mu\mathrm{m}$, $E_1 = 1.3\,\mathrm{MPa}$ and $h_2 = 60\,\mu\mathrm{m}$, $E_2 = 1.3\,\mathrm{MPa}$, respectively.

were video-recorded for the analysis of wavelengths using fast Fourier-transform technique. In the ADCB test (Fig. 3), a PDMS film supported on a thin glass cover slip was brought into contact with another PDMS film supported on a rigid glass plate by inserting a spacer ($100\,\mu\mathrm{m}$) in the open mouth of the crack. The crack front, in this case, led to spontaneous undulation in the form of fingering patterns, the wavelength of which was measured from its video-microscopic image. While the investigations of the instability patterns, *i.e.*, the dependence of the wavelength on the modulus and the thickness of the films, were carried out using both the punch pull-off and the ADCB tests, pull-off force measurements were carried out only with the punch geometry. These measured forces were then compared with the theoretical predictions as discussed in the latter part of the paper. It will be shown that the wavelength of instability is a crucial factor in predicting these punch pull-off forces.

Thin films deposited on rigid substrates were prepared by following the procedure described elsewhere [3,5,20], whereas thin circular PDMS films were prepared using molds with a circular hole (radius 5 mm) through them. Optically smooth, glass disks (radius 4 mm) and glass microscope slides were coated with a self-assembled monolayer (SAM) of hexadecyltrichloro silane (HC). The contact angle of water on the SAM-covered glass surface was 110°.

Figure 4 depicts the wavelengths obtained from the pull-off force experiments and the theoretical results. First, we verify our assumption that the difference between the film/substrate and punch/film configurations is not important in the limit of $a/h_1 \gg 1$ and $a/h_2 \gg 1$. We measured the wavelengths in two different configurations (see inset to Fig. 4a). In Figure 4a, we show that the wavelengths of the instability patterns in both cases of a single

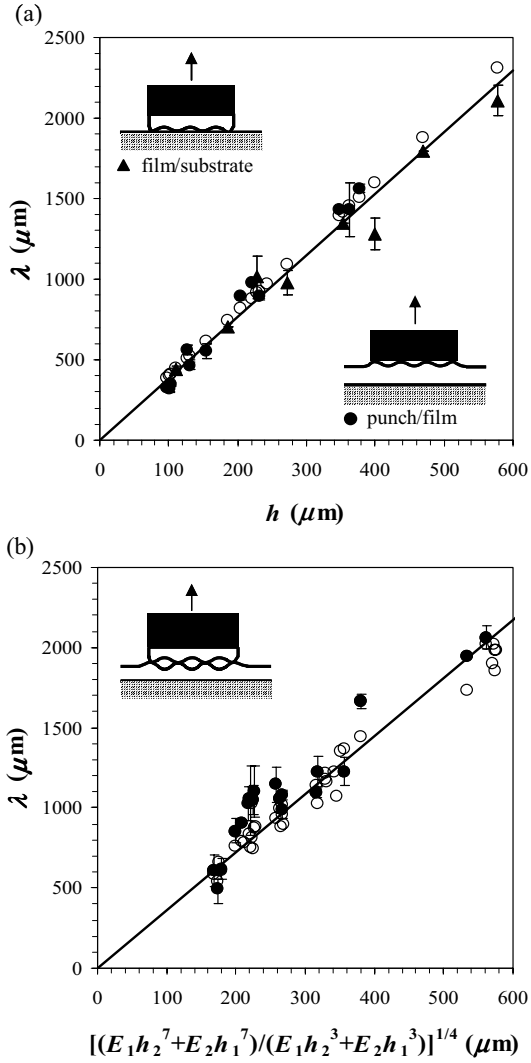


**Fig. 4.** (a) Experimental measurements of wavelengths of the instability patterns and theoretical predictions in two different configurations. Solid triangles and circles correspond to the measured wavelengths in the film/substrate and the punch/film configuration, respectively. The open circles represent the theoretical predictions obtained by multiplying *Case II* results by the proportionality constant 1.3. Although the wavelength of the instability $\lambda$ is proportional to the corresponding film thickness $h$, it is insensitive to the elastic modulus of the film $E$; the solid line is given by $\lambda = 3.8h$ with a correlation coefficient of 0.97. Note that all measurements were made in the condition where $a/h_1 \gg 1$ and $a/h_2 \gg 1$. (b) Plot of the measured wavelengths (•) of the instability $\lambda$ and those (○) predicted by minimization of equation (7) *vs.* the scaled thickness (Eq. (6)). Note that the theoretical predictions were obtained by multiplying the results from *Case II* by 1.3. All the data obey the predicted scaling law and collapse on a single straight line, whose slope is 3.7. The error bars in (a) and (b) represent the standard deviation from the mean values.

film depend linearly on the corresponding film thicknesses. From these results, we conclude that the geometry of the films considered is of minimal significance if $a/h \gg 1$, as expected. Results in Figure 4b on the two-film system

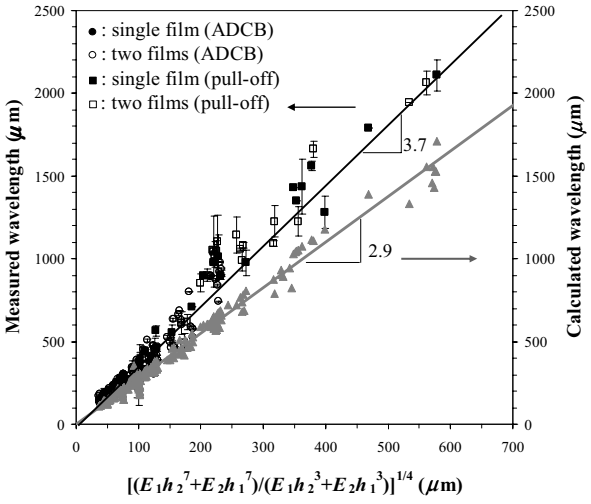


**Fig. 5.** Measured wavelengths of the instability for a variety of film thicknesses ($h_1$ and $h_2 = 40$ to $600\,\mu$m) and elastic moduli ($E_1$ and $E_2 = 1.3$ to $4.8$ MPa) *vs.* theoretical predictions. Note that the data obtained from the ADCB and the pull-off tests fall under one master line. The experimental wavelength varies linearly with the scaled thickness (Eq. (6)) of the films with a correlation coefficient of 0.95 and slope of 3.7. The wavelength (gray triangles) obtained from the *Case II* method also varies linearly with the scaled thickness with a correlation coefficient of 0.98 and slope of 2.9. This indicates that the prefactor of the wavelength predicted by *Case II* is off by a factor of 1.3. Error bars represent the standard deviation of the mean.

show that the experimental values of $\lambda$ over a range of various thicknesses ($h_1$ and $h_2 = 100$ to $600\,\mu$m) and elastic moduli ($E_1$ and $E_2 = 1.3$ to $4.8$ MPa) concur with the scaling relation as shown in equation (6), with a constant of proportionality 3.7 which is essentially the same as that (4) obtained with a single film in contact with a rigid indenter [1,3] in various geometries. The wavelengths obtained in *Case II* are found to be a constant factor smaller than the experimental values. This constant factor was found to be $\sim 1.3$ (see Fig. 5). The open circles of Figures 4a, b represent the theoretical predictions which were obtained by multiplying *Case II* results by the proportionality constant 1.3. It can be observed that both for a single-film configuration (punch/film and film/substrate) and the more general two-film case, the theoretical predictions are in good agreement with the experimental results.

Figure 5 summarizes the instability wavelengths obtained from both the ADCB and the pull-off tests and compares them with the values predicted from the two theoretical approaches. First of all, we note that the wavelengths obtained from both the tests fall nicely on one master line. Secondly, we note that the experimental $\lambda$ correlates quite well with the scaled thickness as predicted by equation (6). The predicted $\lambda$ as obtained from the *Case II* version of the theory also varies linearly with the scaled thickness; however the numerical prefactor is underestimated by a factor of 1.3. These observations suggest that the nature of the instability caused by the forces acting between surfaces during its approach is essentially the same as that when the surfaces are separated, and that the primary factor underlying the instability is the minimization of the shear strain energy in the films.

## 4 Adhesive force in two soft films

Next, we investigate how the pull-off forces between PDMS films of different thicknesses and elastic moduli can be predicted from the instability patterns. Since we observe that the wavelength of instability is considerably larger than the thicknesses of the films, *i.e.*, $\lambda/h_1 > 1$ and $\lambda/h_2 > 1$, equation (5) simplifies to

$$\overline{U}_T \sim \frac{E_1 E_2 \lambda^2 \delta^2}{E_1 h_2^3 + E_2 h_1^3}\,, \tag{15}$$

which leads to the total elastic energy in the film as $U_T = \overline{U}_T \times (\pi a^2)$. The effective spring constant of the film is then

$$k \sim \frac{E_1 E_2 \lambda^2 (\pi a^2)}{E_1 h_2^3 + E_2 h_1^3}\,. \tag{16}$$

Now, using the equation for the pull-off stress as in equation (17), we obtain an expression for the pull-off stress [5] as shown in equation (18):

$$\sigma_c = \sqrt{-\frac{4W_a}{\pi a^3 \left[\dfrac{\partial(1/k)}{\partial a}\right]}}\,, \tag{17}$$

$$\sigma_c \sim \sqrt{\frac{W_a E_1 E_2 \left(E_1 h_2^7 + E_2 h_1^7\right)^{1/2}}{\left(E_1 h_2^3 + E_2 h_1^3\right)^{3/2}}}\,, \tag{18}$$

where $W_a$ is the thermodynamic work of adhesion. Note that for the case of a single film being pulled off from a rigid substrate, equation (18) simply reduces to $\sigma_c \sim (W_a E/h)^{1/2}$, which was previously observed by several authors [5,12,21–25].

Using a home-built apparatus [5], designed along the lines described by Creton *et al.* [9–11], the critical pull-off stresses of several PDMS-coated rigid glass discs from PDMS-coated rigid glass slides were measured. Figures 6a, b summarize the results of these measurements of the critical pull-off stress $\sigma_c$ against $(E/h)^{1/2}$ and equation (18), respectively. All the data agree well with the theoretically predicted scaling law, and are best fitted with a slope of 0.38, consistent with that of the single-film case.

## 5 Conclusion

The main finding of this work is that the surfaces of two soft films become spontaneously rough because of geometric constraint when they come in contact and these interfacial patterns become clearly visible during the

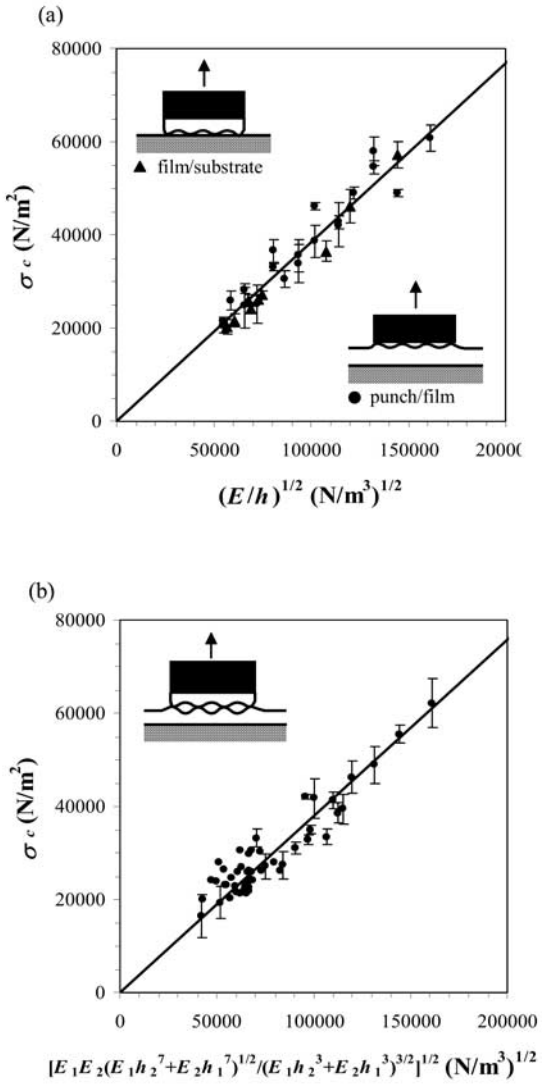


**Fig. 6.** (a) The critical pull-off stresses $\sigma_c$ as a function of $(E/h)^{1/2}$. Solid triangles and circles correspond to the film/substrate and the punch/film configuration, respectively, and the solid line is given by $\sigma_c = 0.39(E/h)^{1/2}$. From the slope and the previous result for a single-film system $\sigma_c = (3.3W_aE/h)^{1/2}$ [5], the thermodynamic work of adhesion $W_a$ was estimated to be 45 mJ m$^{-2}$, which is in good agreement with the reported values [20]. (b) Plot of the critical pull-off stresses $\sigma_c$ in the two-film system *vs.* equation (18). All the data fall on the theoretical prediction and collapse on a single straight line, whose slope is 0.38. The error bars in (a) and (b) represent the standard deviation from the mean values.

separation of films. Despite their differing thicknesses and shear moduli, the two interacting films share the same co-operative instability mode, whose wavelength depends not only on the thicknesses of the films but also on the elastic moduli of the films in a non-linear way. This is in contrast to a single film where the instability mode is independent of the shear modulus and varies linearly with the film thickness. The theoretical scaling laws obtained by a simple energy minimization approach and by the full linear stability analysis of the coupled interfaces are in nice agreement with experimental measurements. The results of this work reveal the important role of surface instability and interfacial cavitation in the problems of adhesion and fracture at soft interfaces, which may also be relevant to the adhesion and debonding of cell membranes that are also intimately involved in cell movement and other functions.

We thank the Office of Naval Research (ONR) and the Pennsylvania Infrastructure Technology Alliance (PITA) for supporting this work. We also thank Animangsu Ghatak for many useful discussions.

## References

1. A. Ghatak, M.K. Chaudhury, V. Shenoy, A. Sharma, Phys. Rev. Lett. **85**, 4329 (2000).
2. K.R. Shull, C.M. Flanigan, A.J. Crosby, Phys. Rev. Lett. **84**, 3057 (2000).
3. A. Ghatak, M.K. Chaudhury, Langmuir **19**, 2621 (2003).
4. W. Mönch, S. Herminghaus, Europhys. Lett. **53**, 525 (2001).
5. J.Y. Chung, M.K. Chaudhury, J. Adhes. **81**, 1119 (2005).
6. J.Y. Chung, M.K. Chaudhury, J. R. Soc. Interface **2**, 55 (2005).
7. V. Shenoy, A. Sharma, Phys. Rev. Lett. **86**, 119 (2001).
8. C.L. Mowery, A.J. Crosby, D. Ahn, K.R. Shull, Langmuir **13**, 6101 (1997).
9. H. Lakrout, P. Sergot, C. Creton, J. Adhes. **69**, 307 (1999).
10. C. Creton, H. Lakrout, J. Polym. Sci. Part B: Polym. Phys. **38**, 965 (2000).
11. A.J. Crosby, K.R. Shull, H. Lakrout, C. Creton, J. Appl. Phys. **88**, 2956 (2000).
12. R.E. Webber, K.R. Shull, A. Roos, C. Creton, Phys. Rev. E **68**, 021805 (2003).
13. S. Poivet, F. Nallet, C. Gay, J. Teisseire, P. Fabre, Eur. Phys. J. E **15**, 97 (2004).
14. S. Poivet, F. Nallet, C. Gay, P. Fabre, Europhys. Lett. **62**, 244 (2003).
15. C.Q. Ru, J. Appl. Phys. **90**, 6098 (2001).
16. V. Shenoy, A. Sharma, Langmuir **18**, 2216 (2002).
17. J. Sarkar, V. Shenoy, A. Sharma, Phys. Rev. E **67**, 031607 (2003).
18. J. Sarkar, V. Shenoy, A. Sharma, Phys. Rev. Lett. **93**, 018302 (2004).
19. J. Sarkar, A. Sharma, V. Shenoy, Langmuir **21**, 1457 (2005).
20. K. Vorvolakos, M.K. Chaudhury, Langmuir **19**, 6778 (2003).
21. K. Kendall, J. Phys. D **4**, 1186 (1971).
22. A.N. Gent, Rubber Chem. Technol. **47**, 202 (1974).
23. F. Yang, J.C.M. Li, Langmuir **17**, 6524 (2001).
24. R.F. Brady jr., I.L. Singer, Biofouling **15**, 73 (2000).
25. I.L. Singer, J.G. Kohl, M. Patterson, Biofouling **16**, 301 (2000).